Vacuum 101 (2014) 306–312

Contents lists available at ScienceDirect

Vacuum

journal homepage: www.elsevier.com/locate/vacuum

End corrections for rarefied gas flows through circular tubes of finite length

Sarantis Pantazis [a,*], Dimitris Valougeorgis [a], Felix Sharipov [b]

[a] Department of Mechanical Engineering, University of Thessaly, Pedion Areos, 38334 Volos, Greece
[b] Departamento de Física, Universidade Federal do Paraná, Curitiba, Brazil

ARTICLE INFO

Article history:
Received 20 July 2013
Received in revised form
25 September 2013
Accepted 26 September 2013

Keywords:
Rarefied gas flows
End effect
Flow rate
Kinetic theory
Vacuum flows
Microflows

ABSTRACT

A method to take into account the influence of the inlet/outlet ends on rarefied gas flows through moderately long capillaries proposed previously [Vacuum **97**, 26 (2013)] is applied to gas flows through circular tubes. The method is based on the concept of effective tube length, representing a sum of its real length and an increment. To calculate the length increment, a flow field near the inlet/outlet of tube is calculated on the basis of the linearized kinetic equation. It is shown that the value of the length increment is independent of the tube length, but depends only on the rarefaction parameter so that it can be used to obtain accurate predictions of the mass flow rate and the axial pressure distribution without great computational effort. Comparisons with results obtained by considering the complete flow domain have shown the efficiency of the end correction concept.

1. Introduction

Most works concerning rarefied gas flows through long capillaries are considered on the basis of linearized kinetic theory for fully developed flow conditions, see e.g. Refs. [1–5]. Such an assumption is justified when the capillary is sufficiently long and the end effects can be neglected. In this case, rarefied gas flow is one-dimensional so that the kinetic equation is significantly simplified and solved with modest computational effort. However, in practical problems of rarefied gas flows through tubes, the end effect may cause a strong deviation from the one-dimensional behavior and hence must be taken into account. In this case, the kinetic equation in its two (or three) dimensional form is solved, see e.g. Refs. [6–11], or the direct simulation Monte Carlo (DSMC) technique is applied, see e.g. Refs. [12–14]. A comparison between the results for flows through short channels obtained by the direct solution of kinetic equations and the DSMC method showed very good agreement [15]. However, both approaches are computationally expensive and impractical, particularly in the case of moderately long capillaries.

Under some conditions, the end corrections may be taken into account by the techniques proposed by the authors previously [16] employing the concept of the effective length [6,2,17–19]. Using an example of gas flow between parallel plates of finite length it was shown that the mass flow rate can be calculated without CPU-time consuming simulations. The condition when the method provides an accuracy of 1% was pointed out in Ref. [16]. The main idea of the effective length concept lies in the consideration of gas flow at the inlet/outlet part of capillary separately from its middle part, where the flow is fully developed. Thus, the kinetic equation is solved near the inlet/outlet of the capillary using fully developed flow as a boundary condition. Furthermore, the effective length values can be tabulated as a function of the rarefaction parameter for future applications.

The objective of the present work is to calculate the length increment for rarefied gas flow through a cylindrical tube using the methodology proposed in Ref. [16] to quantify the influence of the end effects. These data can be used to extend the method of calculation of flow rate through a long tube under arbitrary pressure drop [2,20] to shorter tubes. Even though the approach is based on the linearized kinetic equation, it is shown here that the obtained data can be used for non-linear flows caused by large pressure drops. Such an approach can be easily integrated into practical tools for rarefied gas flows, providing complete solutions for pressure distributions in realistic pipe networks within a few minutes [21].

* Corresponding author. Current address: Physikalisch-Technische Bundesanstalt, 7.54 Vacuum Metrology, Abbestr. 2-12, Berlin 10587, Germany. Tel.: +49 17671568821.
E-mail addresses: sarantis.pantazis@ptb.de, spantazis@mie.uth.gr (S. Pantazis), diva@uth.gr (D. Valougeorgis), sharipov@fisica.ufpr.br (F. Sharipov).

0042-207X/$ – see front matter © 2013 Elsevier Ltd. All rights reserved.
http://dx.doi.org/10.1016/j.vacuum.2013.09.015

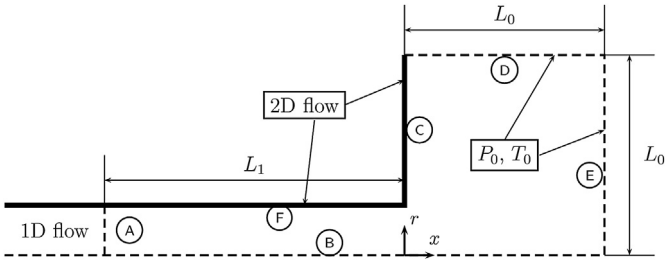

Fig. 1. Flow domain and coordinates.

2. Statement of the problem

Consider a rarefied gas flow at the outlet (or inlet) of a tube and in a container adjacent to the tube as is shown in Fig. 1. Since the gas flow is axisymmetric, it is reasonable to use a cylindrical coordinate system (x,r) with the origin at the center of the junction between the container and tube. Thus, the region $x > 0$ represents the container, while the region $x \le 0$ corresponds to the tube. The gas flows from (or into) the long tube in the x direction into (or from) the infinitely large container, where it is maintained at pressure P_0 and temperature T_0 far from the tube inlet/outlet. Hereinafter, the coordinates (x,r), tube length L and length increment ΔL will be expressed in units of the tube radius R.

It is assumed that inside the tube ($x < 0$), a constant pressure gradient ξ is maintained far from the channel entrance, i.e.

$$\xi = (1/P_0)(\partial P/\partial x) = \text{const at } x \to -\infty. \tag{1}$$

The sign of ξ determines the flow direction: if ξ is positive the gas flows from the container into the tube. Otherwise, the flow direction is opposite. We assume the pressure gradient to be sufficiently small, i.e. $|\xi| \ll 1$, to linearize the kinetic equation.

The expected distribution of pressure along the symmetry axis is shown qualitatively in Fig. 2 under the condition $\xi < 0$. The real pressure P decreases with a constant gradient inside the tube far from the outlet, i.e. at $x < -L_1$, then its shape is changed at the area around $x = 0$ and, finally, it gradually tends to the outlet pressure value P_0. The reference pressure P_R is also depicted in Fig. 2. Its gradient is constant inside the tube ($-L_1 \le x \le 0$) and equal to that of the real pressure far from the outlet, while the pressure P_R is kept equal to the outlet pressure P_0 in the container ($x \ge 0$), i.e. it is given as

$$P_R(x) = \begin{cases} P_0 & \text{at } x \ge 0, \\ P_0(1 + x\xi) & \text{at } x < 0. \end{cases} \tag{2}$$

The pressure difference $\Delta P = P - P_R$ in the tube far from the outlet ($x \le -L_1$) is expected to approach a constant value. It

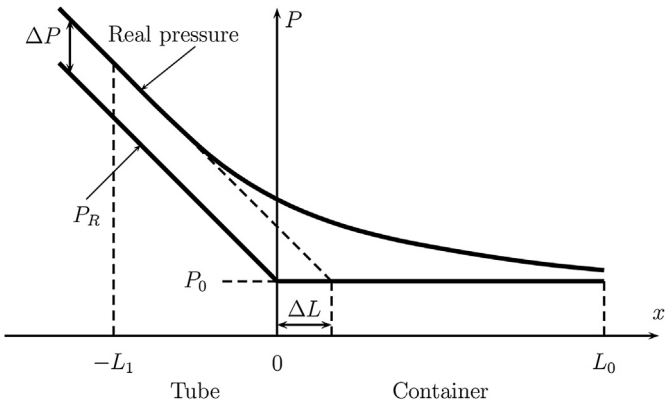

Fig. 2. Pressure distribution and reference pressure in the outlet region.

represents the pressure jump due to the end effect, which can be taken into account by adding the increment ΔL to the tube length. As was shown in our previous paper [16], the length increment is related to the pressure jump as

$$\Delta L = -\Delta P/(\xi P_0). \tag{3}$$

3. Input equations

In order to consider an arbitrary gas rarefaction, the problem is solved on the level of velocity distribution function $f(x,r,\boldsymbol{c})$, which for the problem in question depends on the two coordinates in the physical space, viz., longitudinal x and radial r. The molecular velocity $\boldsymbol{c}$ has the three components: longitudinal c_x, radial c_r, and azimuthal c_φ. Since the pressure gradients ξ is small, the distribution function is linearized using ξ as the small parameter, i.e.

$$f(x, r, \boldsymbol{c}) = f_R[1 + h(x, r, \boldsymbol{c})\xi], \tag{4}$$

where f_R is the reference Maxwellian defined as

$$f_R(x, \boldsymbol{c}) = \frac{n_R(x)}{\pi^{3/2} v_0^3} e^{-c^2}, \quad n_R(x) = P_R(x)/k_B T_0 \tag{5}$$

Here $v_0 = \sqrt{2k_B T_0/m}$ is the most probable molecular velocity, k_B is the Boltzmann constant, T_0 is the equilibrium temperature, m is the molecular mass, n_R is the reference number density having the same profile as that of the reference pressure (2). The molecular velocity $\boldsymbol{c}$ is measured in the units of v_0.

It is convenient to use the cylindrical coordinates for the molecular velocity, i.e. the radial c_r and azimuthal c_φ components of the molecular velocity are presented as

$$c_r = c_p \cos\theta, \quad c_\varphi = c_p \sin\theta. \tag{6}$$

Then the linearized BGK kinetic equation [22] reads

$$c_r \frac{\partial h}{\partial r} - \frac{c_\varphi}{r}\frac{\partial h}{\partial \theta} + c_x \frac{\partial h}{\partial x} + \delta h = \delta\left[\rho + 2\boldsymbol{c}\cdot\boldsymbol{u} + \tau\left(c^2 - \frac{3}{2}\right)\right] + g(x, c_x), \tag{7}$$

where the axial symmetry of the gas flow has been taken into account. The source function g is determined by the reference number density n_R and given as

$$g(x, c_x) = -\frac{c_x}{\xi n_0}\frac{\partial n_R}{\partial x} = \begin{cases} 0 & \text{at } x \ge 0, \\ -c_x & \text{at } x < 0, \end{cases} \tag{8}$$

where Eqs. (2) and (5) have been used. The quantities ρ, $\boldsymbol{u}$, and τ represent the density perturbation, dimensionless bulk velocity and temperature perturbation, i.e.

$$\rho(x, r) = \frac{n(x, r) - n_R}{n_R \xi}, \tag{9}$$

$$\boldsymbol{u}(x, r) = \frac{\widehat{\boldsymbol{u}}(x, r)}{v_0 \xi}. \tag{10}$$

$$\tau(x, r) = \frac{T(x, r) - T_0}{T_0 \xi}, \tag{11}$$

respectively. Here $\widehat{\boldsymbol{u}}$ is the dimensional bulk velocity. These quantities are calculated via the perturbation function as

$$\rho(x,r) = \frac{1}{\pi^{3/2}} \int_{-\infty}^{\infty} \int_{0}^{\infty} \int_{0}^{2\pi} \mathrm{e}^{-c_x^2-c_p^2} h c_p \mathrm{d}\theta \, \mathrm{d}c_p \, \mathrm{d}c_x, \tag{12}$$

$$u_r(x,r) = \frac{1}{\pi^{3/2}} \int_{-\infty}^{\infty} \int_{0}^{\infty} \int_{0}^{2\pi} \mathrm{e}^{-c_x^2-c_p^2} h c_p^2 \cos\theta \, \mathrm{d}\theta \, \mathrm{d}c_p \, \mathrm{d}c_x, \tag{13}$$

$$u_x(x,r) = \frac{1}{\pi^{3/2}} \int_{-\infty}^{\infty} \int_{0}^{\infty} \int_{0}^{2\pi} \mathrm{e}^{-c_x^2-c_p^2} h c_x c_p \mathrm{d}\theta \, \mathrm{d}c_p \, \mathrm{d}c_x, \tag{14}$$

$$\tau(x,r) = \frac{1}{\pi^{3/2}} \int_{-\infty}^{\infty} \int_{0}^{\infty} \int_{0}^{2\pi} \mathrm{e}^{-c_x^2-c_p^2} h \left(\frac{2}{3}c^2 - 1\right) c_p \mathrm{d}\theta \, \mathrm{d}c_p \, \mathrm{d}c_x. \tag{15}$$

Note, the azimuthal component of the bulk velocity vanishes because of the axial symmetry of the flow.

The rarefaction parameter δ determining the solution of Eq. (7) is defined as

$$\delta = RP_0/\mu_0 v_0, \tag{16}$$

where μ_0 is the gas viscosity at the equilibrium temperature T_0. The quantity $l = \mu_0 v_0/P_0$ is the equivalent free path of molecules and the rarefaction parameter is inversely proportional to the Knudsen number. Therefore, the cases $\delta \to 0$ and $\delta \to \infty$ correspond to the free molecular and hydrodynamic limits, respectively.

The integro-differential equations (7), (12)–(15) require a boundary condition for particles entering in the computational domain. According to Fig. 1, the surfaces Ⓕ and Ⓒ are solid and diffuse scattering can be assumed. Mathematically, this means that the perturbation function h of the reflected particles does not depend on the molecular velocity and may be found from the impermeability condition, i.e. $u_r = 0$ on surface Ⓕ and $u_x = 0$ on surface Ⓒ. On the free surfaces Ⓓ and Ⓔ, the incoming molecules correspond to the equilibrium distribution and therefore the perturbation function h is zero. The particles entering through the soft surface Ⓐ have the perturbation

$$h_A(r,c_x,c_p,\theta) = \rho(-L_1,r) + h_1(r,c_x,c_p,\theta), \text{ at } x = -L_1 \text{ and } c_x > 0, \tag{17}$$

where $h_1(r,c_x,c_p,\theta)$ corresponds to the one-dimensional flow obeying the following BGK equation

$$c_r \frac{\partial h_1}{\partial r} - \frac{c_\varphi}{r}\frac{\partial h_1}{\partial \theta} + \delta h_1 = 2\delta c_x u_x - c_x. \tag{18}$$

This equation is subject to the diffuse reflection at the tube wall, i.e. $h_1 = 0$ at $r = 1$ and $c_r < 0$. Details on the numerical procedure to solve such an equation are given in Ref. [23]. Equation (18) is solved once at the beginning of the numerical solution and h_1 is stored in order to be used at each iteration solving Eq. (7). The surface Ⓑ represents the symmetry axis, i.e. the perturbation function h does not depend on the angle θ at $r = 0$. This property is used for the boundary condition at the surface Ⓑ.

Once the kinetic equation (7) is solved, the moments ρ, $\boldsymbol{u}$ and τ are calculated by Eqs. (12)–(15). The length increment ΔL is given by the density asymptotic value far from the tube-container junction and inside the tube, i.e.

$$\Delta L = \lim_{x \to -\infty} \rho(x,r), \tag{19}$$

which follows from Eqs. (1)–(3), (5), and (9), and the state equation $P = nk_BT$. Note, the limit function ρ should not depend on the radial coordinate r in this position.

4. Numerical scheme

The numerical scheme described in Ref. [10] with some improvements has been applied here. The main discretization characteristics are similar to those found in previously formulated discrete velocity schemes [10]. The continuum spectrum of the molecular velocity magnitudes c_p is discretized to M values according to the roots of the Mth order Legendre polynomial mapped in $[0,c_{p,\max}]$, while the molecular velocity angle θ is represented by N_θ values uniformly distributed in the range $[0,2\pi]$. In the physical space, the perturbation function h and its moments ρ, $\boldsymbol{u}$, τ are discretized to $N_x \times N_r$ points according to a second-order scheme. The improvements applied in Ref. [10] regarding memory management and parallelization are also applied here to ensure efficient usage of computational resources. The moments (12)–(15) are calculated by employing Gauss–Legendre quadrature for the velocity magnitudes c_p and c_x and the trapezoidal rule for the angle θ.

The solution algorithm consists of the following steps:

1. The macroscopic quantities ρ, $\boldsymbol{u}$ and τ are initially set equal to zero.
2. The fully developed flow problem (18) is solved in order to be used as the boundary condition for Eq. (7) with the same value of δ.
3. Incoming distributions in cross-section Ⓐ are estimated from Eq. (17) with $c_x > 0$. The value of $\rho(-L_1,r)$ found in the previous iteration (or the one initially assumed) is used.
4. The discretized form of the kinetic equation (7) is solved using a marching scheme.
5. The current iteration is completed by calculating new values for the macroscopic quantities through Eqs. (12)–(15).
6. Steps 3–5 are repeated by updating each time the macroscopic quantities until they have converged, satisfying a predetermined convergence criterion.

The whole process is also repeated for different sizes L_1, L_0 of the computational domain to ensure that their further increase does not change the results with the adopted accuracy. This is evaluated by checking the convergence of the quantities of interest (mostly the pressure perturbation). Upon convergence the quantity $\rho(-L_1,r)$, which is very important for the purposes of the present work, should not depend on r and be constant as we approach the interface boundary Ⓐ.

The iteration scheme is completed when all macroscopic quantities have converged. In our calculations, the average residual per node has been defined as

$$\text{residual} = \frac{1}{4N_{\text{total}}} \sum_{i=1}^{N_{\text{total}}} \left[\left|\rho_i - \rho_i^{pr}\right| + \left|\tau_i - \tau_i^{pr}\right| + \left|u_{x,i} - u_{x,i}^{pr}\right| + \left|u_{r,i} - u_{r,i}^{pr}\right| \right], \tag{20}$$

where the pr superscript denotes the corresponding quantities in the previous iteration and N_{total} is the total number of nodes. An analysis has been performed for the numerical parameters through several runs, resulting in the values given in Table 1 in order to obtain grid independent results. Finally, the computational domain

Table 1
Numerical parameters used in the simulations.

Parameters	Values
Nodes/unit length in dense areas ($N_x = N_r$)	150–200
Discrete angles (N_θ) in (0,2π)	300–400
Discrete magnitudes M for c_x and c_p	16
Max. value of velocity magnitude (c_{max})	5
Convergence criterion	10^{-9}

size parameters (L_1,L_0) are given in Table 2. An increase of the length L_1 is needed when the rarefaction parameter is decreased, while the opposite occurs for the reservoir size L_0. These values were initially selected on the basis of the corresponding parameterization study for the plane geometry [16]. It has been confirmed that they are also sufficient for the tube, given that a smaller L_1 length is required in this case.

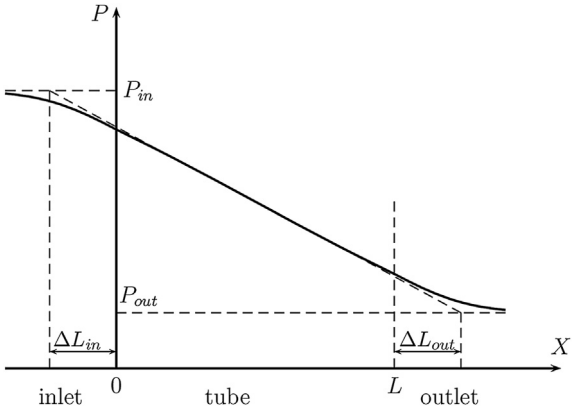

Fig. 3. Pressure distribution along the tube.

5. Effective length increment and corrected flow rate

In order to demonstrate the use of the length increment, let us consider gas flow through a sufficiently long tube of length L measured in radius units connecting two containers. The origin of the longitudinal coordinate X, also measured in radius units, is fixed at the inlet cross section of the tube. The mass flow rate $\dot{M}$ through a long cylindrical tube can be expressed via the Poiseuille coefficient G_P [2] as

$$\dot{M} = -G_P\left(\pi R^2/v_0\right)(\mathrm{d}P/\mathrm{d}X), \tag{21}$$

where $G_P(\delta)$ is a function of the local rarefaction parameter $\delta(X)$ calculated by (16) based on the local pressure $P(X)$, i.e.

$$\delta(X) = RP(X)/(\mu_0 v_0). \tag{22}$$

Numerical data on these coefficients can be found in many previously published papers reviewed in Ref. [2]. Here, we will use the values reported in Ref. [1] based on the BGK model. The global Poiseuille coefficient G [20] is defined via the pressures P_{in} and P_{out} of the gas at the inlet and outlet containers, respectively

$$\dot{M} = G\left[\pi R^2 (P_{in} - P_{out})/v_0 L\right], \tag{23}$$

and determined by the inlet δ_{in} and outlet δ_{out} rarefaction parameters, and by the dimensionless length L, i.e. $G = G(\delta_{in},\delta_{out},L)$. Note, δ_{in} and δ_{out} are calculated by Eq. (16) using P_{in} and P_{out}, respectively. Combining Eqs. (1), (21), (23) and (22), the following relation is obtained

Table 2
Poiseuille coefficient G_P, length increment ΔL and computational domain sizes L_1, L_0 vs rarefaction parameter δ.

δ	G_P, [1]	ΔL	L_1	L_0
0.1	1.4043	1.52	60	10
0.2	1.3820	1.33	60	10
0.4	1.3796	1.16	50	10
0.6	1.3982	1.07	50	10
0.8	1.4261	1.01	40	12
1	1.4594	0.964	40	12
2	1.6608	0.841	30	12
4	2.1188	0.735	30	15
6	2.5999	0.704	20	15
8	3.0894	0.688	20	15
10	3.5821	0.682	20	15
∞		0.681[a]		

[a] Hydrodynamic limit, Ref. [24].

$$G\mathrm{d}X = -[L/(\delta_{in} - \delta_{out})]G_P(\delta)\mathrm{d}\delta. \tag{24}$$

The expected pressure distribution $P(X)$ along the tube and in the containers is depicted in Fig. 3 which shows that the pressures at the inlet ($X = 0$) and outlet ($X = L$) cross sections are not equal to P_{in} and P_{out}, respectively. Pressures jumps occur at these positions due to the end effects, which can be taken into account by the length increments, i.e. the pressures P_{in} and P_{out} may be taken to correspond to the points $X = -\Delta L_{in}$ and $X = L + \Delta L_{out}$, respectively. Thus, the integration of the right-hand-side of Eq. (24) from δ_{out} to δ_{in} corresponds to the integration of the left side from $L + \Delta L_{out}$ to $-\Delta L_{in}$ with respect to X. Then, the relation of $G(\delta_{in},G_{out},L)$ to $G_P(\delta)$ is obtained as

$$G(\delta_{in},\delta_{out},L) = \frac{L}{(L + \Delta L_{in} + \Delta L_{out})(\delta_{in} - \delta_{out})}\int_{\delta_{out}}^{\delta_{in}} G_P(\delta)\mathrm{d}\delta. \tag{25}$$

In the particular case of the small pressure difference, i.e. $(P_{in} - P_{out}) \ll P_{in}$, the rarefaction parameters δ_{in} and δ_{out} are equal to each other and then Eq. (25) is reduced to

$$G(\delta,L) = \frac{L}{L + 2\Delta L}G_P(\delta), \tag{26}$$

where $\delta = \delta_{in} = \delta_{out}$ and $\Delta L = \Delta L_{in} = \Delta L_{out}$. In fact, Eqs. (25) and (26) are the same as those obtained in our previous work [16] for a plane channel, but the values of G_P, ΔL_{in} and ΔL_{out} are different.

When the flow rate G is known, the pressure distribution is calculated by integrating Eq. (24) from $X = -\Delta L_{in}$ up to an arbitrary X. Then using the relation (22) we obtain the function $X = X(P)$ in the form

$$X = \frac{L}{(P_{in} - P_{out})G}\int_{P_{in}}^{P} G_P\left(\frac{\delta_{in}}{P_{in}}P\right)\mathrm{d}P - \Delta L_{in} \tag{27}$$

which is inverted into $P = P(X)$. In the particular case of small pressure difference, the pressure distribution is linear

$$P(X) = P_{in} + \frac{X + \Delta L}{L + 2\Delta L}(P_{in} - P_{out}). \tag{28}$$

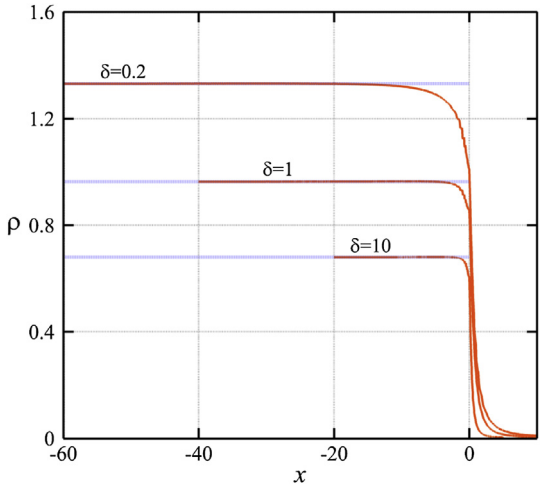

Fig. 4. Density perturbation profile along the symmetry axis $r = 0$: solid lines – numerical solution, dotted lines – limit value.

6. Results and discussion

Based on this methodology, the effective length increment ΔL has been calculated as a function of the rarefaction parameter δ. As has been shown above (Eq. (19)), the length increment ΔL is a limit value of the density perturbation ρ which should be constant far from the tube end. This characteristic is verified in Fig. 4 where the density perturbation along the symmetry axis ($r = 0$) is shown for $\delta = 0.2, 1$ and 10. It is seen that as $x \to -L_1$, the density perturbation ρ indeed approaches to a constant value. Near the tube outlet ($x = 0$), the perturbation ρ drastically drops and then vanishes at $x \to L_0$.

The same quantity and streamlines are plotted in Fig. 5 in two-dimensional contours for the area close to $x = 0$ and the same values of δ. Inside the tube ($x < 0$), the density field progressively becomes one-dimensional, i.e. ρ is constant in each cross section and the streamlines are parallel far from $x = 0$ inside the tube.

The values of the length increment ΔL are presented in Table 2 for various values of δ covering a wide range of the gas rarefaction. It is observed that the values of ΔL are monotonically decreased by increasing δ. Such a behavior indicates that the end effect is more significant for highly rarefied flows. These results are qualitatively similar to those obtained previously for the plane geometry [16]. In the hydrodynamic limit ($\delta \to \infty$), the increment ΔL tends to the value 0.681 obtained from the Navier–Stokes equation in Ref. [24]. In the opposite limit, i.e. $\delta \to 0$, the length increment ΔL tends to infinity. The numerical data for the small values of δ indicate the following asymptotic behavior of the increment

$$\Delta L = 0.9 - 0.27 \ln \delta \quad \text{at } \delta \to 0. \tag{29}$$

A comparison between the results obtained by the present approach with those based on the consideration of the complete flow field without any decomposition [8–11] and used here as the benchmark solution will allow us to test the accuracy and limitations of the end correction approach in the whole range of the gas rarefaction. The dimensionless flow rate G in case of small pressure drop, calculated by Eq. (26) employing the results for G_P and ΔL from Table 2 is presented in Table 3 for several values of the rarefaction parameter δ and aspect ratio L. The data obtained by considering the complete domain of the flow [10] are also given in this Table for comparison. Note, the results reported in Ref. [9] are in a good agreement with those from Ref. [10]. The relative difference $\Delta G/G$ between Eq. (26) and the exact results [10] is given in the

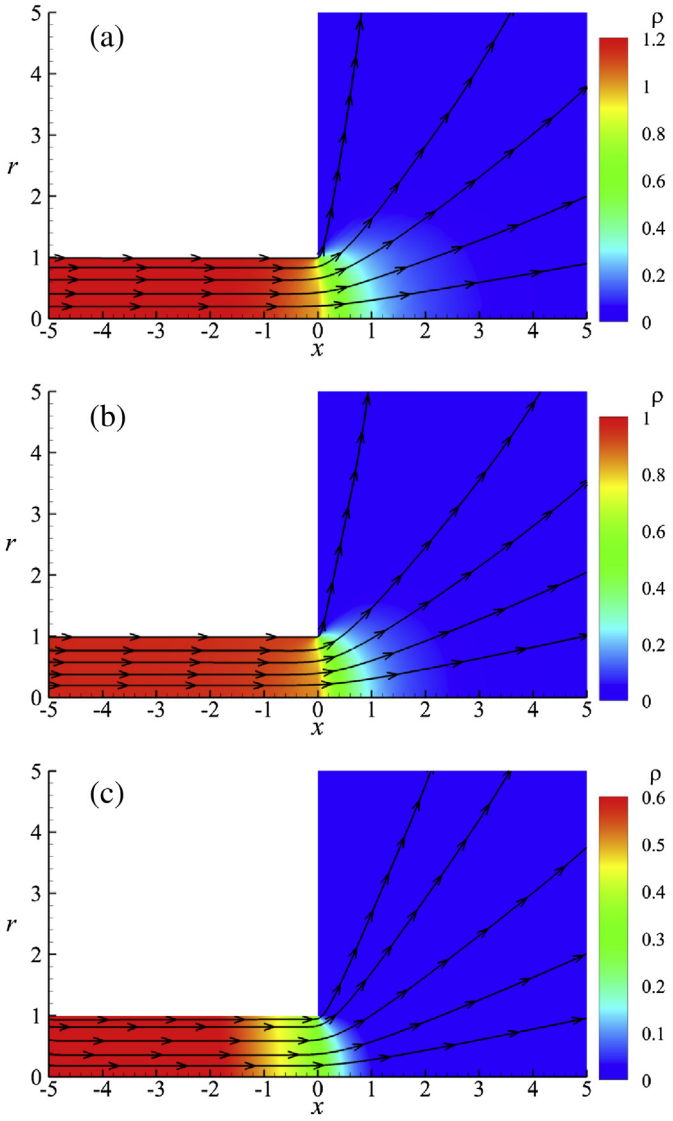

Fig. 5. Density perturbation distributions and streamlines: (a) $\delta = 0.2$, (b) $\delta = 1$, (c) $\delta = 10$.

fifth column of Table 3. The quantity $2\Delta L/L$ characterizing the contribution of the end effect into the whole resistance of tube is given in the last column of the same Table. It can be seen that for a rather long tube, i.e. $L \geq 5$, the end correction approach provides practically the same results as those obtained exactly. It is rather surprising that the approach works also for the short tubes, i.e. $L = 1$ and 2, in the transitional ($\delta = 1$) and hydrodynamic ($\delta = 10$) regimes even when the length increment is larger than the tube length, i.e. $2\Delta L/L > 1$. Only near the free-molecular regime ($\delta = 0.1$) and for short tube ($L \leq 2$) the approach error reaches 11%.

When the pressure drop in the tube ends is large, i.e. $P_{in} \gg P_{out}$, then Eq. (25) containing two values of the length increment, viz. ΔL_{out} and ΔL_{in} should be used. Numerical values of the coefficient G calculated from Eq. (25) for some combinations of L, δ_{in} and P_{out}/P_{in} are given in Table 4. The values of G calculated directly considering the whole flow domain in Ref. [11] are also given in the same Table. It should be noted that the complete domain results [11] were obtained from the ES kinetic model [25]. However, a comparison of these results with those based on the BGK model showed that the difference does not exceed 2.6%. The relative difference $\Delta G/G$ between the end correction approach and exact calculation is given in

Table 3
Dimensionless flow rate G for small pressure difference obtained by Eq. (26) and that calculated considering the complete flow domain in Ref. [10], relative differences $\Delta G/G$ between these results and end correction $2\Delta L/L$ vs the tube length L and gas rarefaction δ.

L	δ	G		$\Delta G/G$	$2\Delta L/L$
		Eq. (26)	Ref. [10]		
1	0.1	0.348	0.393	0.11	3.04
	1	0.498	0.503	0.01	1.93
	2	0.619	0.621	0.00	1.68
	10	1.52	1.48	−0.02	1.36
2	0.1	0.557	0.598	0.07	1.52
	1	0.743	0.745	0.00	0.96
	2	0.902	0.902	0.00	0.84
	10	2.13	2.099	−0.01	0.68
5	0.1	0.873	0.891	0.02	0.61
	1	1.05	1.05	0.00	0.39
	2	1.24	1.24	0.00	0.34
	10	2.81	2.79	0.01	0.27
10	0.1	1.08	1.08	0.01	0.30
	1	1.22	1.22	0.00	0.19
	2	1.42	1.42	0.00	0.17
	10	3.15	3.13	0.01	0.14
20	0.1	1.22	1.22	0.00	0.15
	1	1.33	1.33	0.00	0.10
	2	1.53	1.53	0.00	0.08
	10	3.35	3.34	0.00	0.07

Table 4
Dimensionless flow rate G for large pressure drop obtained by Eq. (25) and that calculated considering the whole flow domain in Ref. [11], relative differences $\Delta G/G$ between these results and the total end correction $\Delta L_{tot}/L$ ($\Delta L_{tot} = \Delta L_{in} + \Delta L_{out}$) vs the tube length L, gas rarefaction δ and pressure ratio P_{out}/P_{in}.

L	δ_{in}	P_{out}/P_{in}	G		$\Delta G/G$	$\Delta L_{tot}/L$
			Eq. (25)	Ref. [11]		
5	1	0.1	0.94	0.98	0.04	0.50
5	2	0.1	1.04	1.07	0.02	0.43
5	10	0.1	1.87	1.68	0.11	0.33
5	1	0.5	1.01	1.03	0.01	0.42
5	2	0.5	1.16	1.17	0.01	0.36
5	10	0.5	2.32	2.25	0.03	0.28
10	1	0.1	1.13	1.16	0.03	0.25
10	2	0.1	1.23	1.25	0.02	0.22
10	10	0.1	2.13	2.06	0.04	0.16
10	1	0.5	1.19	1.20	0.01	0.21
10	2	0.5	1.33	1.34	0.01	0.18
10	10	0.5	2.60	2.58	0.01	0.14
20	1	0.5	1.30	1.31	0.01	0.10
20	10	0.5	2.77	2.77	0.00	0.07

the sixth column of Table 4. The contribution of the end effect $(\Delta L_{in} + \Delta L_{out})/L$ into the resistance of the tube is given in the last column of the same Table. It can be seen that for a large pressure drop the method proposed here also works well. The maximum difference between the end correction approach and the exact calculation is 11% at $L = 5$, $\delta_{in} = 10$ and $P_{out}/P_{in} = 0.1$ that can be explained by the existance of shock waves in the downflow container under these conditions [13]. For all other combinations, the difference does not exceed 4% even when the contribution of the end effect is about 50%. It is noted that such a comparison is not possible in the case of expansion into vacuum ($P_{out} = \delta_{out} = 0$) since the development length L_1 in this case is infinite according to Eq. (29).

The numerical results [9,10] for the complete domain of the flow due to a small pressure drop confirm the linear pressure distribution (Eq. (28)). It is more interesting to compare the pressure distribution when its drop is large, e.g. $P_{out}/P_{in} = 0.5$. In this case, the distributions $P(X)$ were calculated by Eq. (27) for the length $L = 5$ and for the rarefaction parameter $\delta = 1$ and 10. The results are plotted in Fig. 6 and compared with those obtained in Ref. [11] by considering the complete flow domain. It can be seen that the distribution $P(X)$ is practically linear and in a good agreement with the exact results for $\delta = 1$. The pressure profile $P(X)$ is slightly different from the straight line for $\delta = 10$. In this case, the difference between Eq. (27) and the exact distribution is larger, but the approximate approach still provides reasonable results.

Based on the results presented in Tables 2–4, some general remarks on the applicability range of the end correction approach are drawn which may be considered as guidelines for engineering purposes. Compared to the case of no end effect consideration, the introduction of the end effect correction will always improve the accuracy of the simulations. Since its implementation is very simple, it is recommended to apply the end correction in the whole range of gas rarefaction δ and for any pressure ratio P_{out}/P_{in} when the ratio of the end correction length over the tube length is larger than 0.01 ($\Delta L/L > 0.01$). Of course, for small pressure differences with $L \leq 1$ and for large pressure differences with $L \leq 5$ the introduced error may be significant (over 10%) and it is recommended to apply the DSMC method or the direct solution of a kinetic equation in the whole domain of the gas flow in order to obtain accurate results. The above statements define approximately the upper and lower length limits of a tube of moderate length.

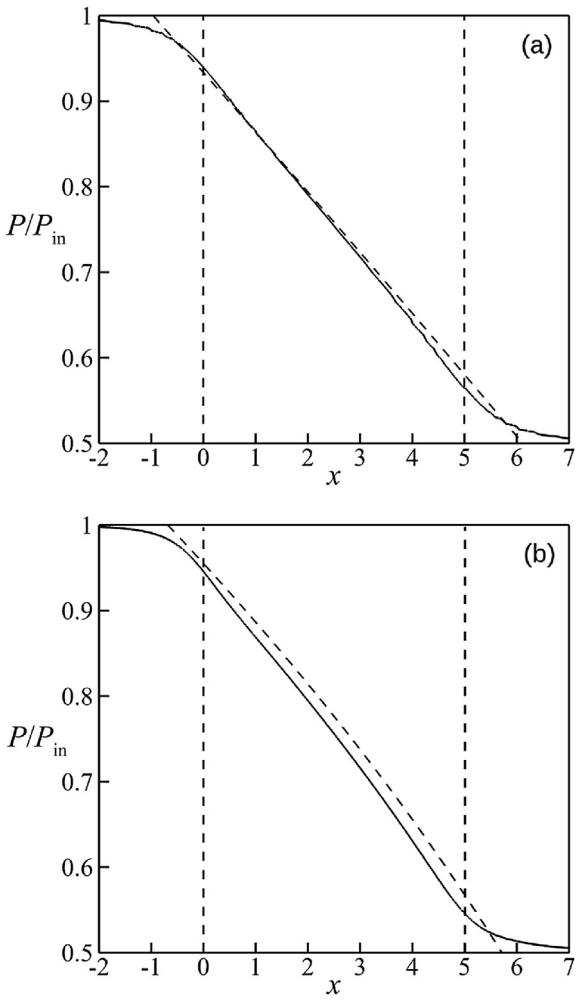

Fig. 6. Pressure distribution along the symmetry axis at $L = 5$ and $P_{out}/P_{in} = 0.5$: solid line – solution for the complete flow domain [11], dashed line – solution obtained by Eq. (27); (a) $\delta = 1$, (b) $\delta = 10$.

7. Conclusions

The method to take into account the influence of the inlet/outlet ends on rarefied gas flows through moderately long capillaries proposed previously in Ref. [16] has been applied to gas flows through circular tubes. According to the method, the effective tube length represents a sum of its real length and an increment related to the flow field near the inlet/outlet of tube. Such an approach allows us to calculate the flow rate and flow field through circular tubes with modest computational effort. Numerical results of the length increments based on the BGK model equation and diffuse gas–surface interaction have been obtained for several values of the gas rarefaction. Comparisons with results obtained by including the whole flow domain have shown the efficiency of the end correction concept. It has been shown that the end correction method works well even for relatively short tubes. The effective length increment values given here can be used in practical applications with minimal computational effort.

Acknowledgments

The authors (S.P. and D.V.) acknowledge support by the Association Euratom – Hellenic Republic. The views and opinions expressed herein do not necessarily reflect those of the European Commission. The author (F.Sh.) thanks the Brazilian Agency CNPq for the support of his research. Simulations have been partially performed at the supercomputing facility in Jülich, Germany.

References

[1] Cercignani C, Sernagiotto F. Cylindrical Poiseuille flow of a rarefied gas. Phys Fluids 1966;9(1):40–4.
[2] Sharipov F, Seleznev V. Data on internal rarefied gas flows. J Phys Chem Ref Data 1998;27(3):657–706.
[3] Sharipov F. Application of the Cercignani–Lampis scattering kernel to calculations of rarefied gas flows. III. Poiseuille flow and thermal creep through a long tube. Eur J Mech B/Fluids 2003;22:145–54.
[4] Varoutis S, Naris S, Hauer V, Day C, Valougeorgis D. Computational and experimental study of gas flows through long channels of various cross sections in the whole range of the Knudsen number. J Vac Sci Technol A 2009;27(1):89–100.
[5] Titarev VA, Shakhov EM. Nonisothermal gas flow in a long channel analyzed on the basis of the kinetic S-model. Comput Math Math Phys 2010;50(12):2131–44.
[6] Akinshin VD, Makarov AM, Seleznev VD, Sharipov FM. Rarefied gas motion in a short planar channel over the entire Knudsen number range. J Appl Mech Tech Phys 1989;30(5):713–7.
[7] Aristov VV, Frolova AA, Zabelok SA, Arslanbekov RR, Kolobov VI. Simulations of pressure-driven flows through channels and pipes with unified flow solver. Vacuum 2012;86(11):1717–24.
[8] Titarev VA, Shakhov EM. Computational study of a rarefied gas flow through a long circular pipe into vacuum. Vacuum 2012;86(11):1709–16.
[9] Titarev VA. Rarefied gas flow in a circular pipe of finite length. Vacuum 2013;94:92–103.
[10] Pantazis S, Valougeorgis D. Rarefied gas flow through a cylindrical tube due to a small pressure difference. Eur J Mech B/Fluids 2013;38:114–27.
[11] Pantazis S. Simulation of transport phenomena in conditions far from thermodynamic equilibrium via kinetic theory with applications in vacuum technology and MEMS. Ph.D. Volos, Greece: University of Thessaly; 2011.
[12] Varoutis S, Valougeorgis D, Sazhin O, Sharipov F. Rarefied gas flow through short tubes into vacuum. J Vac Sci Technol A 2008;26(2):228–38.
[13] Varoutis S, Valougeorgis D, Sharipov F. Simulation of gas flow through tubes of finite length over the whole range of rarefaction for various pressure drop ratios. J Vac Sci Technol A 2009;22(6):1377–91.
[14] Varoutis S, Day C, Sharipov F. Rarefied gas flow through channels of finite length at various pressure ratios. Vacuum 2012;86(12):1952–9.
[15] Sharipov F. Benchmark problems in rarefied gas dynamics. Vacuum 2012;86(11):1697–700.
[16] Pantazis S, Valougeorgis D, Sharipov F. End corrections for rarefied gas flows through capillaries of finite length. Vacuum 2013;26:26–9.
[17] Shakhov EM. Linearized two-dimensional problem of rarefied gas flow in a long channel. Comput Math Math Phys 1999;39(7):1192–200.
[18] Shakhov EM. Rarefied gas flow in a pipe of finite length. Comput Math Math Phys 2000;40(4):618–26.
[19] Titarev VA, Shakhov EM. Efficient method of solution of a problem of rarefied gas flow in a planar channel of large finite length. Comput Math Math Phys 2012;52(2):269–84.
[20] Sharipov F, Seleznev V. Rarefied gas flow through a long tube at any pressure ratio. J Vac Sci Technol A 1994;12(5):2933–5.
[21] Misdanitis S, Valougeorgis D. Design of steady-state isothermal gas distribution systems consisting of long tubes in the whole range of the Knudsen number. J Vac Sci Technol A 2011;29(6):061602.
[22] Bhatnagar PL, Gross EP, Krook MA. A model for collision processes in gases. Phys Rev 1954;94:511–25.
[23] Sharipov F. Rarefied gas flow through a long tube at any temperature difference. J Vac Sci Technol A 1996;14(4):2627–35.
[24] Weissberg HL. End correction for slow viscous flow through long tubes. Phys Fluids 1962;5(5):1033–6.
[25] Holway LH. New statistical models for kinetic theory: method of construction. Phys Fluids 1966;9:1658.